

Mapping the South Atlantic Anomaly continuously over 27 years

P.C. Anderson ^{a,*}, F.J. Rich ^b, Stanislav Borisov ^c

^a W. B. Hanson Center or Space Sciences, University of Texas at Dallas, 800 W Campbell Rd. MS WT15, Richardson, TX 75080-3021, USA

^b M.I.T. Lincoln Laboratory, Group 97, 244 Wood Street, Lexington, MA 02421, USA

^c Université Catholique de Louvain Center for Space Radiations, Building Marc de Hemptinne, Chemin du Cyclotron, 2, B-1348, Louvain-la-Neuve, Belgium

ARTICLE INFO

Keywords:

South Atlantic Anomaly
Radiation belts
Energetic electrons and protons

ABSTRACT

The South Atlantic Anomaly (SAA) is a region of reduced magnetic intensity where the inner radiation belt makes its closest approach to the Earth's surface. Satellites in low-Earth orbit pass through the SAA periodically, exposing them to several minutes of strong radiation each time, creating problems for scientific instruments, human safety, and single event upsets (SEU). For the first time, we are able track the SAA movement continuously over 27 years, using overlapping satellites in similar orbits with similar instruments. The Defense Meteorological Satellite Program (DMSP) spacecraft have been carrying the Special Sensor J (SSJ) precipitating energetic particle spectrometers since 1982. The instruments are susceptible to MeV electrons and protons that pass through the spacecraft skin and instrument case and get counted. This "background" is easily identified and we use it to map the movement of the SAA. Comparison with energetic particle data from the Energetic Particle Telescope (EPT) instrument on the Proba-V spacecraft indicates that the best match with the SSJ data occurs in the energy range above about 2.6 MeV for electrons and above about 29 MeV for protons. The peak flux and extent of the SAA from both the SSJ and EPT instruments are nearly identical in longitude while in latitude, the peak EPT flux is 5° south of the peak SSJ flux. However, the shapes of the SAA in latitude and the locations of the outer radiation belts are nearly identical. We find that the SAA moves 0.06° N/yr and 0.28° W/yr. We also find a difference with the movement and location of the SAA from the contamination by high energy particles on the Special Sensor Ultraviolet Spectrographic Imager (SSUSI) instrument on DMSP F16 (Shaefer et al., 2016). However, the SSUSI instrument is located on the opposite side/bottom of the spacecraft and Shaefer et al. (2016) estimated that most of the particle noise pulses in the SSUSI instrument are produced by protons greater than about 45 MeV. Thus the contamination in the SSUSI instrument is produced by a different population of particles than the contamination in the SSJ/5 instrument which would lead to differences in movement and location of the SAA. While this study focuses on the SAA movement on a yearly basis, further analysis will allow us to investigate the movement on shorter time scales, the variation of the flux intensity, the spatial extent of the SAA, and the dynamics of the outer radiation belt.

1. Introduction

The SAA (Kurnosova et al., 1962) is a region of weakened geomagnetic field centered in southeast South America. Because of the weakened magnetic field, inner radiation belt particles can mirror at lower altitudes increasing the local particle flux. It is thus the region where the inner radiation belt makes its closest approach to the Earth's surface. Satellites in low-Earth orbit pass through the SAA periodically, exposing them to several minutes of strong radiation each time: the International Space Station requires extra shielding to deal with this problem and astronauts on extravehicular activity try to avoid it. The energetic increased particle

flux can also produce 'glitches' or noise in astronomical data. For instance, the Hubble Space Telescope is turned off when passing through the SAA. It can cause problems in on-board electronic systems - single event upsets (SEUs), cause premature aging of computer, detector and other spacecraft components, and is said to be the cause of peculiar 'shooting stars' seen in the visual field of astronauts. Fig. 1 shows the location of a number of SEUs observed on the UoSAT-2 spacecraft in 1988 and 1989 (Underwood, 1990). Also plotted are the geomagnetic field strength contours at 700 km (the spacecraft altitude) for the year 1989 as calculated by the International Geomagnetic Reference Field (IGRF) geomagnetic field model. It is very clear that most of the SEUs

* Corresponding author.

E-mail addresses: phillip.anderson1@utdallas.edu (P.C. Anderson), frederick.rich@ll.mit.edu (F.J. Rich), stanislav.borisov@uclouvain.be (S. Borisov).

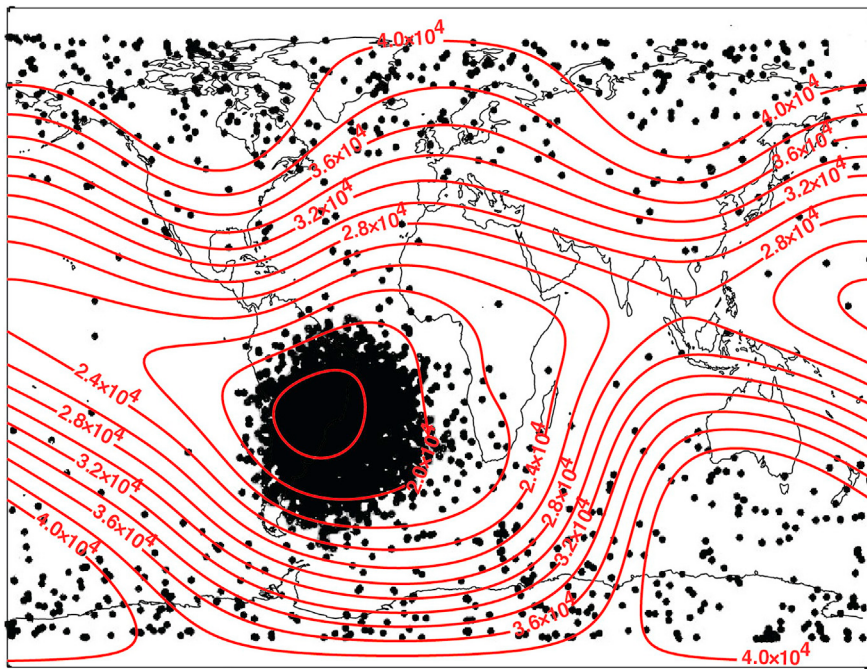


Fig. 1. The location of a number of SEUs observed on the UoSAT-2 spacecraft in 1988 and 1989. The red lines are contours of geomagnetic field strength at 700 km and the numbers indicate the strength of the magnetic field in nT. [adapted from Underwood (1990)]. (For interpretation of the references to color in this figure legend, the reader is referred to the Web version of this article.)

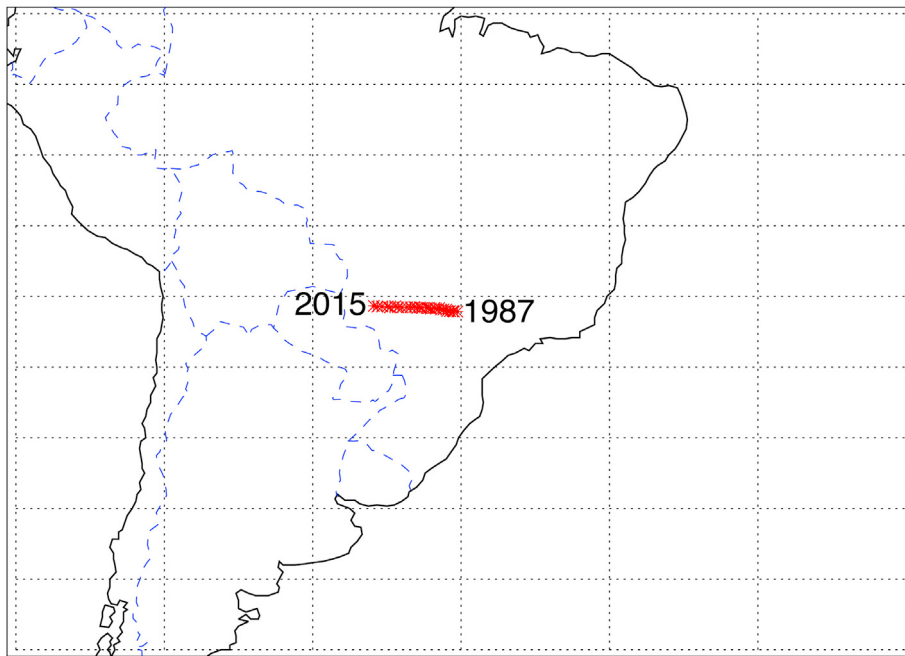


Fig. 2. The location of the geomagnetic field minimum for the years of 1988 through 2015.

occur within the SAA (the other geographically distributed SEUs are likely caused by galactic cosmic rays). It is thus very important to understand the dynamics of the SAA and how the variation in the Earth's geomagnetic field and the radiation belts affects the strength and location of the energetic particle fluxes.

At present the strength of the Earth's magnetic field is decreasing by about 5% every hundred years (Merrill and McElhinny, 1983); in the SAA, the strength of the magnetic field is decreasing ten times as fast. The location of the minimum geomagnetic field within the SAA is also known to show a secular variation with time, associated with the changing of the

magnetic moment, moving steadily westward and northward. Fig. 2 shows the yearly variation of the geomagnetic field minimum as calculated by the epoch appropriate IGRF at 800 km (the nominal altitude of our energetic particle measurements) for the years of 1988 through 2015. The movement is not exactly linear in latitude and longitude (indeed there are also short term variations); the movement is approximately 0.204° GLON west and 0.13° GLAT north per year. While the location of the peak in energetic particle flux is close to the geomagnetic field minimum, it also depends on the particle distribution in the radiation belts, the energy of the observed particles, and the altitude of

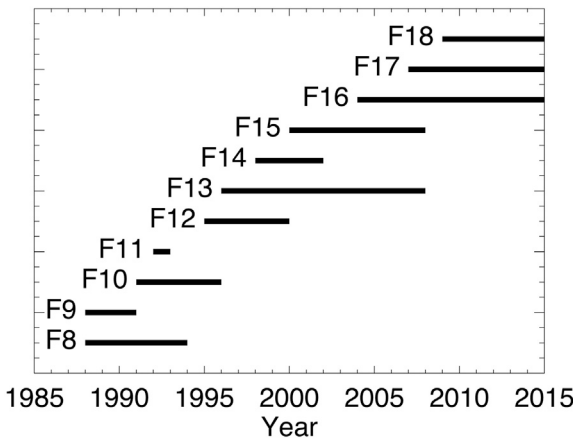


Fig. 3. The coverage of the DMSP satellites for 1988 through 2015, restricted to periods when the data was available for the entire year.

observations. Notice in Fig. 1 that the peak in the location of the SEUs is not at the minimum in the geomagnetic field. A number of studies have mapped the SAA using a diverse set of instruments over several decades (e.g., Badhwar, 1997; Ginet, 2006; Grigoryan et al., 2008; Fürst et al., 2009; Casadio and Arino, 2011; Schaefer et al., 2016). However, there are large differences in the results due to, among other factors, the variety of instruments and their calibration, the energy of the observed particles, the orbital dynamics of the various spacecraft, and the wide range of mission durations. For instance, both Jones et al., (2017) and Ye et al., (2017) used data from SAMPEX (Solar Anomalous and Magnetospheric Particle Explorer) spacecraft to study the secular variation of the SAA

over several years. Jones et al., (2017) used the Low Energy Ion Composition Analyzer (LICA) instrument which measures $\sim 0.5\text{--}5$ MeV/nucleon ions while Ye et al., (2017) used the Proton/Electron Telescope (PET) which measures protons in the 18–250 MeV range and electrons in the energy range from approximately 0.4 to ~ 30 MeV. Jones et al., (2017) found the average drift speed of the SAA peak to be $0.20 \pm 0.04^\circ$ per year westward and $0.11 \pm 0.01^\circ$ per year northward while Ye et al., (2017) noted that the drift speed was highly dependent on the energy of the measured protons. They both found a significant variation in the location of the SAA with proton energy, with the peak flux of protons in the energy range from 70.5 to 500 MeV being a much as 15° south of the peak flux in 19–37.4 MeV protons.

Stassinopoulos et al., (2015) provides an excellent review of many of the results, limited to an altitude of 800 km, coincidentally the altitude (or nearly so) that the DMSP spacecraft operate at. Quoting Stassinopoulos et al., (2015): “In most papers from the SAA literature, data from experiments unrelated to the SAA were used. The primary interest and concern of the authors of these papers appeared to be the drift of the SAA and the effects of the SAA’s radiation on LEO missions. As a result, an unexpectedly large spread in the derived SAA drift rates was observed. These unusual findings could be due to the great variety in acquisition methods, to the criteria used for the selection of data, and to the data processing techniques. The result is that the SAA drift values appear to be spread over an abnormally large range. Specifically, the minimum drift rate reported is 0.170/yr W and 0.080/yr N, and the maximum drift rate reported is 0.660/yr W and 0.220/yr N.”

In our study, we use data from the energetic particle instruments on the Defense Meteorological Satellite Program (DMSP) F8 — F18 satellites to track the movement of the SAA over a 27-year period, providing for the first time continuous monitoring of the SAA from a single altitude and

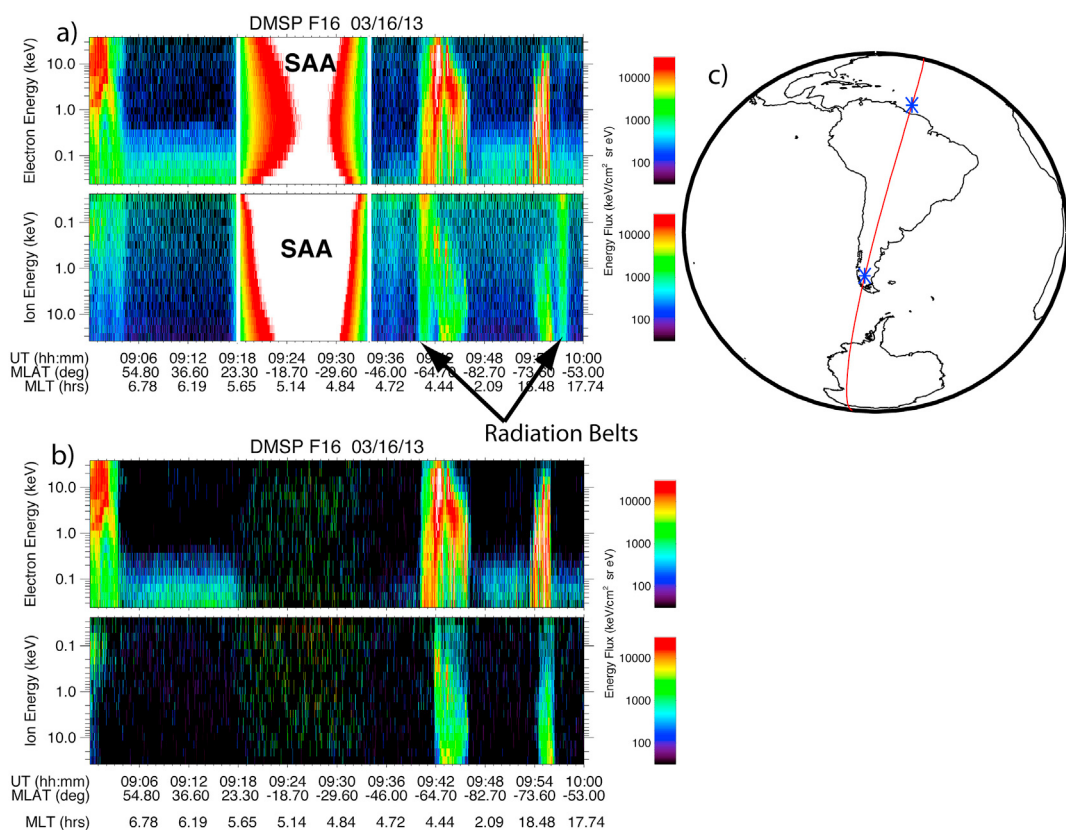


Fig. 4. Electron (top) and ion (bottom) color spectrograms from the DMSP F16 SSJ/5 instrument before (a) and after (b) the contamination from high energy particles within the SAA and the outer radiation belt have been removed. Fig. 4c shows the ground track of the spacecraft; the asterisks indicate the location of the identified edges of the SAA, as indicated by the vertical white lines in (a). (For interpretation of the references to color in this figure legend, the reader is referred to the Web version of this article.)

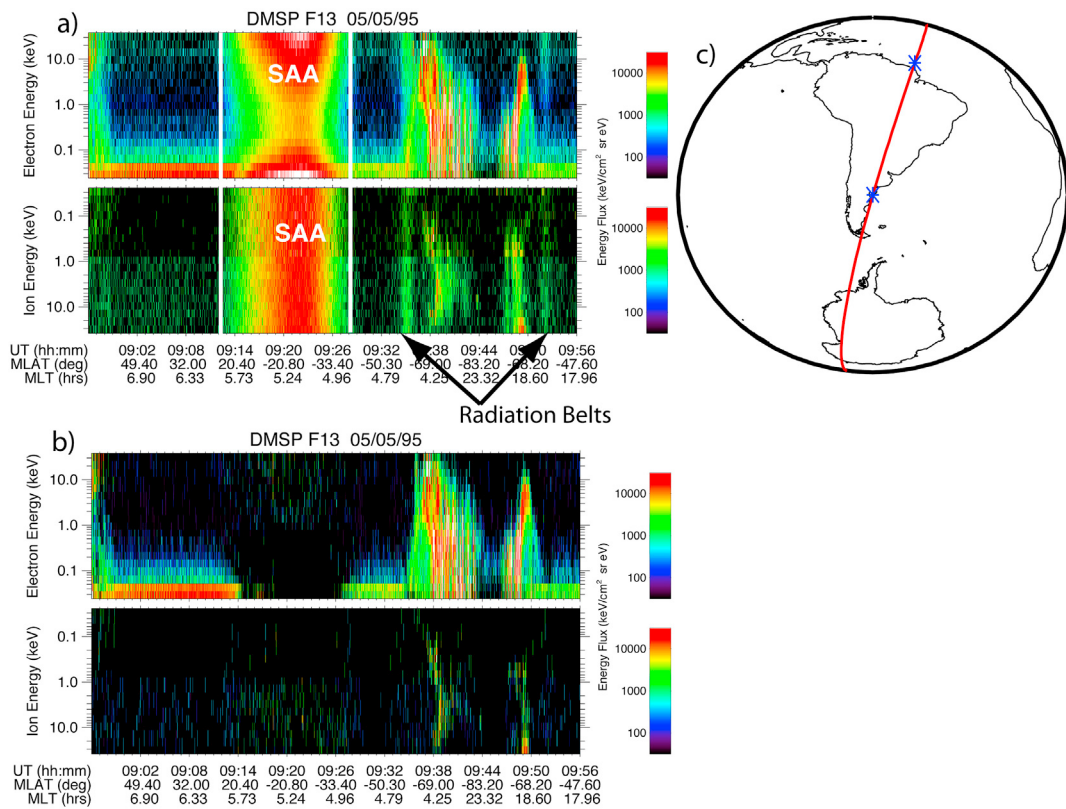


Fig. 5. Electron and ion spectrograms from the DMSP F13 spacecraft in the same format as Fig. 4.

from intercalibrated instruments making the same measurements for such an extended period.

2. DMSP satellites and instruments

The DMSP spacecraft are a set of Air Force meteorological satellites first launched in the 1960s to originally primarily provide cloud cover imagery. They fly in circular, sun-synchronous orbits, at nominally 840 km, and 99° inclination, with orbital periods of ~101 min. Their ascending nodes are typically near 1800 and 2000 h solar local time (SLT) although that varies somewhat with satellite and with time as the orbit altitude decays due to atmospheric drag. Because of the nature of this polar orbit, the spacecraft fly through the SAA seven to eight times per day.

DMSP F6 was the first satellite to begin monitoring the space environment, carrying precipitating ion and electron spectrometers and a thermal plasma monitor. F7 and all spacecraft after and including F12 carried magnetometers. Starting with F16, the spacecraft began carrying two UV imagers for monitoring the aurora, the ionosphere and the neutral atmosphere. For our study we focus on the spectrometers (SSJ/4 and SSJ/5) on F8 through F18 covering the years from 1988 to 2015. Fig. 3 shows the coverage of all the satellites for that period, restricted to periods when the data was available for the entire year. There were at least two spacecraft and as many as four always in orbit furnishing data throughout this period, providing a total of 71 years of data.

The instruments of interest for this study are the SSJ/4 (F8 — F15) and SSJ/5 (F16 — F18). Both instruments provide the precipitating electron and ion fluxes in 19 energy channels ranging from 30 eV to 30 keV, although they are slightly different instruments. The SSJ/4 consists of four Channeltron detectors, one each for high energy (1 keV–30 keV) electrons and ions and one each for low energy (30 eV–1 keV). Each detector has a pair of cylindrical curved plates which electrostatically deflect the particles as they pass from the aperture to the detector, with a complete sweep occurring every second. The

measurements are centered on local vertical within a solid angle of 2° by 5° for the high energy channels and 4° by 5° for the low energy channels. For a complete description of the SSJ/4 instrument, see Hardy et al., (1984). In contrast, the SSJ/5 consists of a pair of nested triquadrispherical (270°) electrostatic analyzers with a field of view of 4° by 90° ranging from zenith to the horizon divided into six 15° zones. Micro-channel plates are then used to amplify and transform single ion or electron events into charge pulses. The electron and ion counts from all six zones are then summed once per second to provide output similar to the SSJ4 other than the differing field of view. A similar instrument using nested triquadrispherical electrostatic analyzers was the Shuttle Potential and Return Electron Experiment (SPREE) instrument flown on the Tethered Satellite System (TSS)-1 space shuttle experiment (Oberhardt et al., 1994).

What makes these instruments useful for investigating the SAA is that MeV particles are capable of penetrating the sides of the instrument case and reaching the Channeltron detectors and microchannel plates. This “contamination” produces a nearly constant count rate in all channels. The count rate can be used as a proxy for the flux of energetic electrons and protons and indeed this contamination is actually used as a standard to determine and correct for the degradation of the instruments (see McFadden et al., 2007 for a complete description of the process). A data processing routine developed by Ernest Holman of Air Force Research Laboratory (AFRL) removes the contamination by looking for a nearly constant count rate in the higher energy channels of the electron or ion spectrum. If such a nearly constant count rate is found, then that rate plus one sigma of the rate is subtracted from all counts in the given spectrum. We use that subtracted count rate as a proxy for the flux of energetic electrons in the SAA (and the outer radiation belt) as will be demonstrated.

3. Methodology

Fig. 4a and b shows an examples of the SSJ/5 data from the DMSP F16

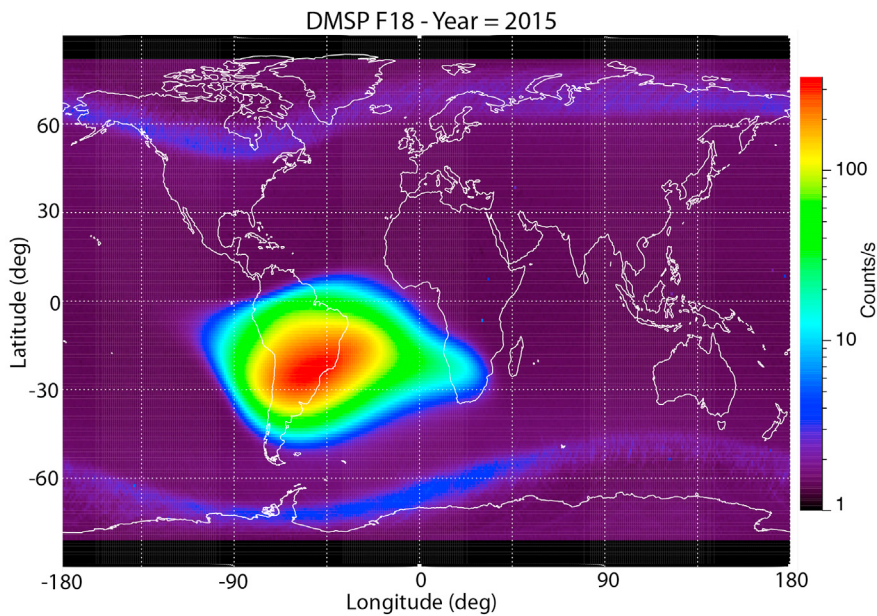


Fig. 6. Geographic map of the removed contamination (counts/s) in the DMSP F18 SSJ/5 electron detectors binned and averaged in 1° GLAT by 1° GLON bins for the year 2015.

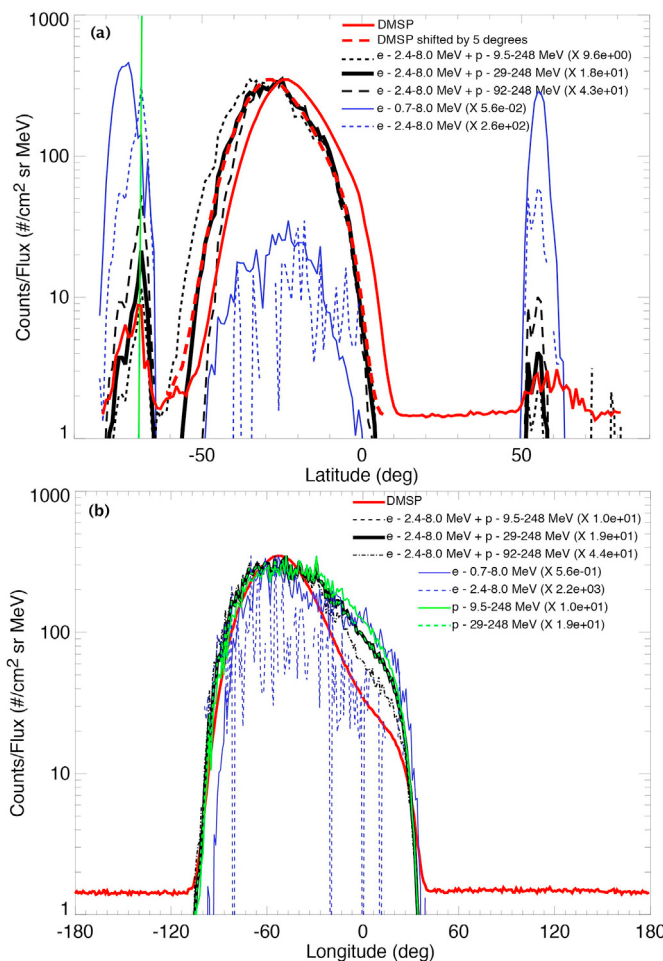


Fig. 7. (a) The SSJ/5 fluxes and EPT fluxes in various energy ranges (indicated in the upper right corner of the figure) against latitude along the longitude of the location of the peak SSJ/5 flux. (b) The SSJ/5 fluxes and EPT fluxes in various energy ranges (indicated in the upper right corner of the figure) against longitude along the latitude of the peak SSJ/5 flux.

spacecraft before (a) and after (b) the contamination was removed by the Holeman algorithm. The top two spectrograms show the electron (top) and ion (bottom) color spectrograms for passes from the northern auroral oval, through the SAA, and across the southern auroral oval. Note that in the ion spectrograms, energy is plotted from top to bottom on the Y axis. The contamination from high energy particles within the SAA and the outer radiation belt are clearly seen in the spectrograms in Fig. 4a. (White indicates a saturation of the color scale, not a saturation in the instrument.) Note that the contamination does not appear in the figure as a constant flux across all energies because each energy channel has a different geometric factor. The image to the right shows the ground track of the spacecraft; the asterisks indicate the location of the identified edges of the SAA, indicated by the white vertical lines in Fig. 4a. Fig. 4b shows the data after the correction has been applied and the flux in the SAA and in the outer radiation belt has been removed. The intense fluxes in the lower energies are due to photoelectrons and are also removed within the SAA by the algorithm. We thus do not use the removed contamination in the lower three energy channels in our analysis.

Fig. 5a and b shows examples of the SSJ/4 data from the DMSP F13 spacecraft in the same format as Fig. 4. Notice that the Channeltrons in the SSJ/4 instrument are less susceptible to the contamination than the microchannel plates on the SSJ/5 instruments. There is considerable overlap between the satellites with SSJ/4 and SSJ/5 instruments (see Fig. 2 showing, for example, that F13 and F15 overlap with F16 and F17 for several years) allowing the instruments to be intercalibrated for future studies of the variation in the SAA size and intensity; we focus only on the location of the centroid of the SAA for this study which is not impacted by these differences. Again note the removal of the flux in the SAA and the radiation belts.

To perform our analysis and determine the centroid of the SAA, we binned the removed contamination (counts/s) in the electron detectors in 1° geographic latitude (GLAT) by 1° geographic longitude (GLON) bins, and averaged the number of counts/s in each bin by dividing the total counts/s by the number of measurements in that bin. We performed the binning for each year, for each satellite from 1988 to 2015 and plotted the results on a geographic map. Fig. 6 shows an example of one of these maps for the DMSP F18 spacecraft for the year 2015. The SAA is clearly delineated as are the outer radiation belts in both the northern and southern hemisphere. We do not know necessarily the energy of the electrons and protons producing the contamination but can get an idea of

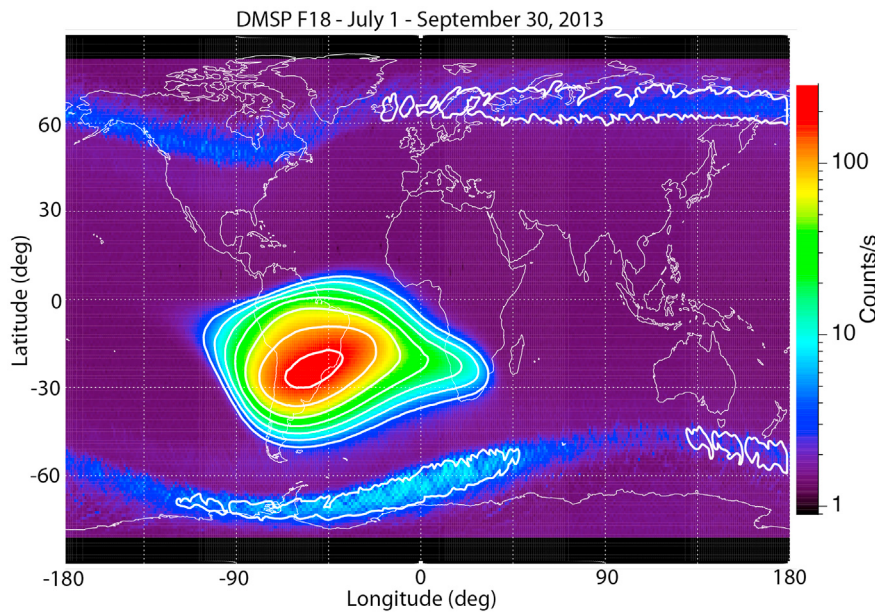


Fig. 8. Geographic map of the removed contamination (counts/s) in the DMSP F18 SSJ/5 electron detectors plotted in the same format as Fig. 6. The data is from a 3-month period from July 1, 2013 to September 30, 2013. The thick white lines are contours of constant counts/s.

their energy by comparing our maps with maps produced by other instruments measuring the radiation belt particles on satellites in similar low-Earth orbits. One example of such a satellite is the European Space Agency (ESA) spacecraft Proba-V which carries the Energetic Particle Telescope (EPT). The EPT is an ionizing particle spectrometer that measures He-ion fluxes between 38 and 1 200 MeV, proton fluxes in the energy range 9.5–300 MeV, and electron fluxes in the energy range 0.5–20 MeV. Proba-V was launched in May 2013 into a nearly circular orbit at 820 km, with a 98.7° inclination and 10:30–11:30 SLT descending node. So its orbit is nearly identical to DMSP making it the ideal satellite to compare measurements with. For a complete description of the EPT instrument, see [Cynamukungu et al., \(2014\)](#).

To perform the comparison, we selected a 3-month period from July 1, 2013 to September 30, 2013 and binned both the DMSP SSJ/5 data from F18 and the Proba-V EPT data in 1° GLAT by 1° GLON bins. We determined the latitude and longitude of the peak flux in the SSJ/5 data (see below for a discussion of the method) and plotted the SSJ/5 fluxes and EPT fluxes in various energy ranges against latitude along the longitude (Fig. 7a) of the location of the peak SSJ/5 flux and against longitude along the latitude (Fig. 7b) of the location of the peak flux. The solid red line in Fig. 7a shows the SSJ/5 fluxes while the blue lines show the EPT electron fluxes from 0.7 MeV to 8.0 MeV (solid lines) and 2.4–8.0 MeV (dashed lines) as indicated in the upper right had corner of the figure. (Data from the EPT for electrons greater than 8.0 MeV is not used as it is only an approximation of the fluxes in the 8–20 MeV energy range due to nonuniform efficiencies in that channel.) The Y-axis scale is for SSJ/5 counts/s and the EPT fluxes are multiplied by a scaling factor (shown in the parenthesis) for plotting purposes. The outer radiation belts are clear at high latitudes in the northern and southern hemispheres. However, the match with the SSJ/5 data is much better for electrons in the 2.4–8.0 MeV range both in location and relative flux in opposite hemispheres. In the southern hemisphere, the location of the peak fluxes in both the EPT and SSJ/4 are nearly identical and show the same shape (the peaks in the SSJ/5 and EPT fluxes, indicated by the green line, are nearly perfectly co-located) while the peak fluxes in the 0.7 MeV–8.0 MeV are located further south and do not show the same shape. Also note that the ratio of the peak fluxes in the northern and southern outer radiation belts in the 2.4–8.0 MeV range are much closer to the SSJ/5 ratio than the ratio in the 0.7 MeV–8.0 MeV range. This gives us confidence that the contamination in the SSJ instruments from

electrons is caused by electrons with energies greater than about 2.4 MeV.

However, the flux in the SAA as measured by the SSJ/5 instrument is much larger than the flux in the outer radiation belts (by an order of magnitude) while the fluxes at all energies in the EPT electrons are much larger in the outer radiation belts. Thus energetic protons must contribute significantly to the SSJ/5 contamination in the SAA (the outer radiation belts are populated almost exclusively with electrons). To examine the energy of the protons producing the contamination, we summed the EPT fluxes from the electrons in the 2.4–8.0 MeV range and the protons in various energy ranges. Plotted in the black lines are the fluxes from the electrons and protons in the 9.5–248 MeV range (small dashed lines), 29–248 MeV range (solid lines), and 92–248 MeV range (large dashed lines). The best comparison with the SSJ/5 data occurs for the 29–248 MeV range (plus 2.4–8.0 MeV electrons). The poleward extend of the SAA (and the peak) increases with energy such that it is over 10° poleward for protons in the 92–248 MeV range vs protons in the 9.5–248 MeV range, in agreement with the results of [Jones et al., \(2017\)](#) and [Ye et al., \(2017\)](#). The equatorward extent of the SAA is nearly identical for all energies. But the location of the SAA measured by the SSJ/5 is equatorward of the SAA for all energies measured by the EPT. However, if we shift the SSJ/5 data by 5° south (dashed red lines) we find that the width and latitudinal shape of the SAA is nearly identical with the shape of the SAA in the proton energy range of 29–248 MeV range (plus 2.4–8.0 MeV electrons).

Fig. 7b shows the data in the same format as Fig. 7a but against longitude instead of latitude. We also plotted the flux of only protons in the 9.5–248 MeV and 29–248 MeV ranges. For all energies, the longitudinal extent of the SAA is nearly identical and agrees with the extent measured by the SSJ/5. However, the SSJ/5 data shows a dropout in fluxes in the eastern extent of the SAA not seen in the EPT data.

So the comparison of the SSJ/5 data and the EPT data gives us confidence that the contamination in the SSJ/5 instrument is caused by electrons with energies greater than about 2.4 MeV and protons greater than about 29 MeV. One reason for the differences in the SAA location in latitude and the flux dropout in longitude could be the lack of electron measurements at higher energies than 8 MeV. A better quantification of these energy ranges will be difficult and require further investigation; this is planned as a future project.

Fig. 8 shows the SSJ/5 data from July 1, 2013 to September 30, 2013

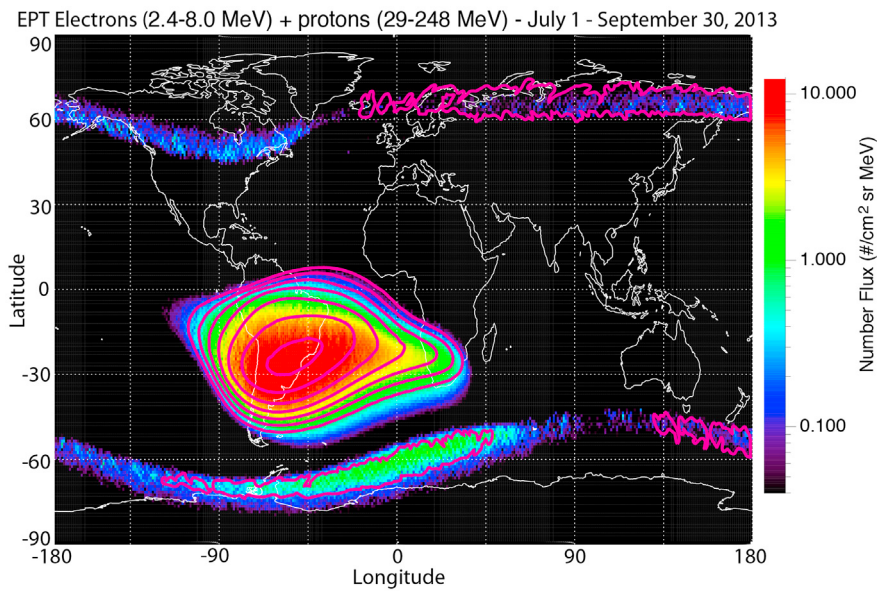


Fig. 9. The Proba-V EPT electrons fluxes in the energy range 2.6–8.0 MeV and proton fluxes in the energy range 29–248 MeV binned and plotted in a similar format to Fig. 6 and 7 for DMSP F18. The constant count contours from Fig. 8 are plotted on top of the Proba-V maps.

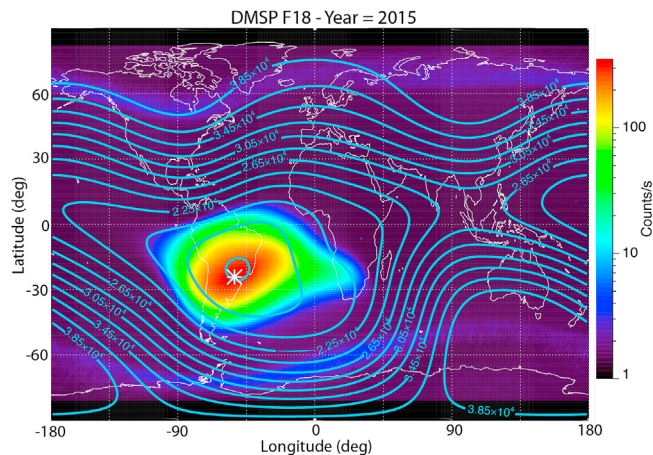


Fig. 10. The same map and data as in Fig. 6 but this time with contours of the geomagnetic field magnitude calculated by the epoch appropriate IGRF model at 800 km. The white asterisk indicates the location of the peak flux.

on a geographic map in a similar format to Fig. 6 but with contours of constant counts/s delineating the SAA and the more intense portions of the outer radiation belts. We then plotted the sum of the EPT proton data in the energy range of 29–248 MeV range and the electron data in the 2.4–8.0 MeV range as shown in Fig. 9 in a similar format and overlaid the SSJ/5 flux contours from Fig. 8. It is clear that there is a very close correspondence in the location of the radiation belts as identified by the two instruments while the shape and location of the SAA in longitude is also very similar but the location in latitude measured by the EPT is south of the location measured by the SSJ/5.

To identify and map the movement of the SAA, we produced a yearly map for each DMSP satellite similar to those shown in Figs. 6 and 8; at times we had up to three satellites concurrently operating (see Fig. 3). We thus produced 67 maps for the years of 1988 through 2015. To identify the location of the peak electron flux in the SAA, for each yearly map for each satellite we produced contours for successively larger values of bin counts/s (1 count/s steps), thus producing smaller contour areas, similar to the contours in Fig. 8 (only closer). We then calculated the centroid of last smooth, continuous contour, and identified the latitude and

longitude of the centroid as the center of SAA. The centroid was computed as the weighted average of each of the midpoints of the lines in the region encompassed by the contour. The weights used were proportional to the length of the lines. Thus we acquired 67 peak SAA locations over the 27 years encompassed by this study.

4. Results and discussion

As mentioned in the introduction, while the location of the peak in energetic particle flux is close to the geomagnetic field minimum, it also depends on the particle distribution in the radiation belts, the energy of the observed particles, and the altitude of the observations. This is clearly illustrated in Fig. 10 which shows again the results from F18 in 2015 illustrated in Fig. 6 but this time with contours of the geomagnetic field magnitude calculated by the epoch appropriate IGRF model at 800 km for 2015. The white asterisk indicates the location of the peak flux determined as described above. While the minimum in the geomagnetic field magnitude within the SAA is close to the maximum in the particle fluxes, it is slightly north and west. So, while the location and movement of the particle fluxes in the SAA are expected to be similar to the secular variation the geomagnetic field, it is critical to investigate their relationship for energetic particles of different species and energies at different altitudes for extended periods of time.

The next 6 figures, Fig. 11a, b, and c and Fig. 12a, b, and c, show examples of the results for several satellites distributed over time every five years (except for 1988–1995) from 1988 to 2015. The data in Fig. 11a, b, and c are from the SSJ/5 and the data in Fig. 12a, b, and c are from the SSJ/4, thus the different scales and slightly different looks. Contours of constant flux are shown in each figure along with the white asterisk showing the identified flux peak. While the intensity and shape of the SAA (and the radiation belts) is seen to change over time, the centroid in each case is easily identified. The movement over time can clearly be seen when comparing the six figures. Note that the flux (see the color bar to the left of the plots) is lower for F13 and F8; this is of course because the data is from the SSJ/4 instruments which, as noted previously, is less susceptible to the contamination.

Fig. 13a and b shows the results of our analysis. Fig. 13a shows the identified latitude of the SAA centroid and Fig. 13b shows the longitude. While there does appear to be some non-linear motion over time, the movement is relatively linear and the red lines show linear fits to the data. The results of the fits are that the SAA moves $0.277 \pm 0.008^\circ$

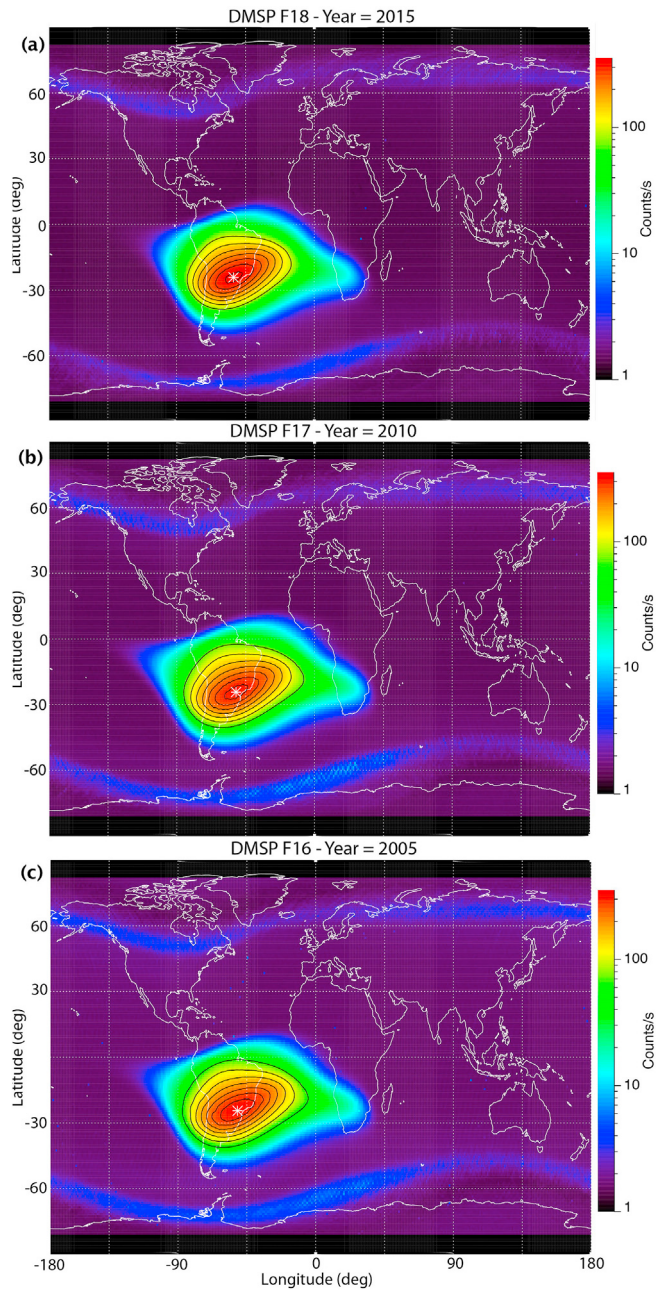


Fig. 11. Geographic maps of the removed contamination (counts/s) in the (a) DMSP F18 SSJ/5 electron spectrometer in 2015, (b) DMSP F17 SSJ/5 in 2010, and (c) DMSP F16 SSJ/5 in 2005 with over plotted contours and peak flux indicated by the white asterisks.

westward per year and $0.064 \pm 0.008^\circ$ northward. As mentioned in the introduction, there is a wide range of published results on the SAA movement; the westward movement is within the range of published values while the northward movement is on the low side of published values. Fig. 14 shows the movement on a map of South America (blue asterisks); included is the location of the minimum in the magnetic field at 800 km (red asterisks) as shown in Fig. 2. While both show similar trends, the peak in energetic electron flux is south and east of the minimum in the geomagnetic field. The movement however, is similar.

We would note that Schaefer et al., (2016) performed a similar analysis of the movement of the SAA using the DMSP F16 spacecraft. However, they used particle noise pulses in the photomultiplier of the Special Sensor Ultraviolet Spectrographic Imager (SSUSI) on the spacecraft. Although they used one of the spacecraft used in our analysis, their

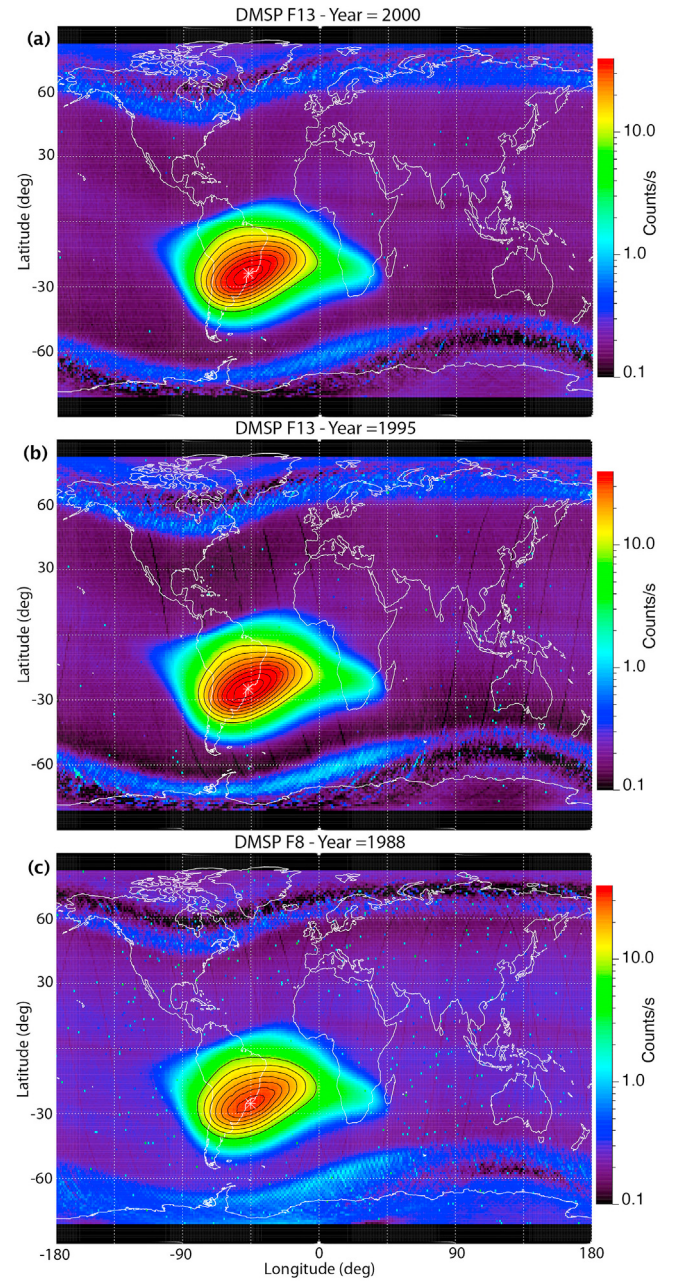


Fig. 12. Geographic map of the removed contamination (counts/s) in the (a) DMSP F13 SSJ/4 electron spectrometer in 2000, (b) DMSP F13 SSJ/4 in 1995, and (c) DMSP F8 SSJ/4 with over plotted contours and peak flux indicated by the white asterisks.

results are somewhat different showing a longitude drift of $0.36 \pm 0.06^\circ$ W/yr, and latitude drift of $0.16 \pm 0.09^\circ$ N/yr. They also show a substantially different location for the peak fluxes. For instance, in 2005, they find an SAA centroid of 45.62° W GLON and -23.97° GLAT while for the same satellites and the same year (see Fig. 12), we find a centroid of 49.92° W GLON and -24.28° GLAT, significantly west and north of their location. The instruments are in different locations on the spacecraft: SSUSI is on the earthward/bottom on the spacecraft while the SSJ/5 is on the top, thus they do experience a different population of particles. And of course they are different instruments with different responses to the contamination. Schaefer et al., (2016) estimate that most of their particle noise pulses in the SSUSI instrument are produced by protons greater than about 45 MeV. As the distribution of particle fluxes in the SAA and the secular movement of the SAA are dependent on the

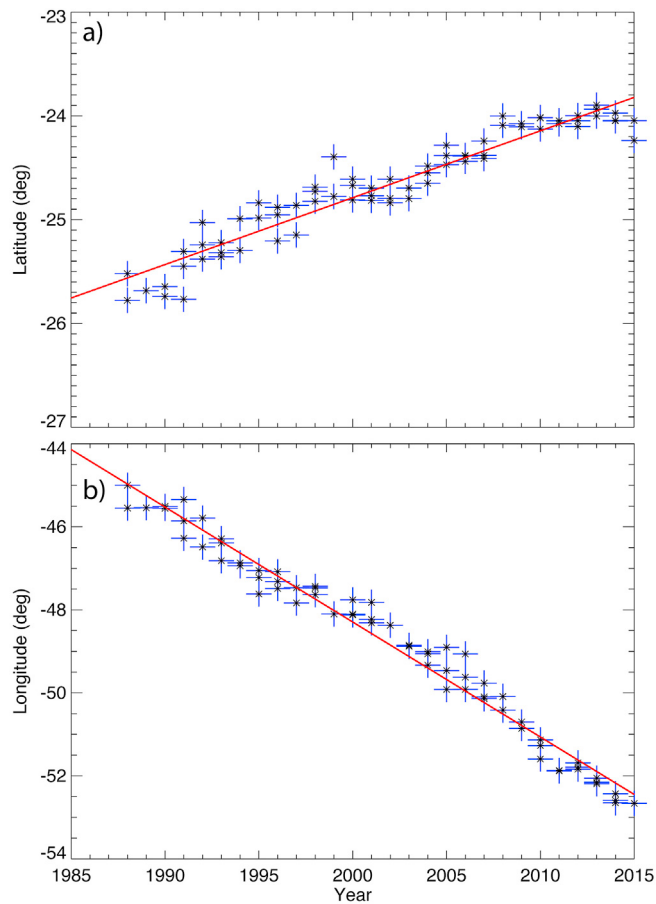


Fig. 13. The identified latitude (a) and longitude (b) of the SAA centroid. The red lines are linear fits to the data. (For interpretation of the references to color in this figure legend, the reader is referred to the Web version of this article.)

particle distribution in the radiation belts and the energy of the observed particles, it would be expected that the locations determined by the contamination in the SSUSI and SSJ/5 instruments would be different.

5. Conclusions

We have used the contamination from MeV electrons in the DMSP SSJ/4 and SSJ/5 energetic auroral particle spectrometers to track the movement of the SAA over a 27-year period from 1988 to 2015. The multiple, overlapping satellites used (DMSP F8 — F18) provided a continuous, uninterrupted monitoring of the SAA over that period. This is the first time such a long term analysis has been possible using satellites in similar orbits with similar instruments. MeV particles in the SAA (and the outer zone radiation belts) penetrate the sides of the spectrometer cases, reaching the Channeltron detectors and microchannel plates and produce a nearly constant count rate in all channels. This contamination is easily detected and removed; however, we used this signal to map the SAA by binning the detected counts/s in 1° GLAT by 1° GLON bins in year-long periods and averaging. Comparing with measurements by the EPT instrument on the Proba-V, which flies in a nearly identical orbit to DMSP, we were able to determine that the contamination in the SSJ/5 instruments is likely caused by electrons with energies greater than about 2.6 MeV and protons with energies greater than about 29 MeV.

We determined the peak in the energetic particle flux in the SAA by plotting the data on a geographic map, and drawing contours for successively larger values of bin counts/s (smaller contour area), and calculated the centroid of last smooth, continuous contour to identify the latitude and longitude of the center of SAA. Due to the overlapping satellite coverage, we ended up with 67 SAA location identifications over the 27-year period. The resultant locations showed that the SAA moves $0.277 \pm 0.008^\circ$ westward per year and $0.064 \pm 0.008^\circ$ northward. The peak in energetic electron flux was systematically located south and east of the minimum in the geomagnetic field as determined by the epoch appropriate IGRF model but with a relatively similar movement: 0.204° west per year and 0.13° northward for the geomagnetic minimum.

Schaefer et al., (2016) performed a similar analysis of the movement of the SAA using the SSUSI ultraviolet image on the DMSP F16 spacecraft and found substantially different drifts and locations for the SAA peak.

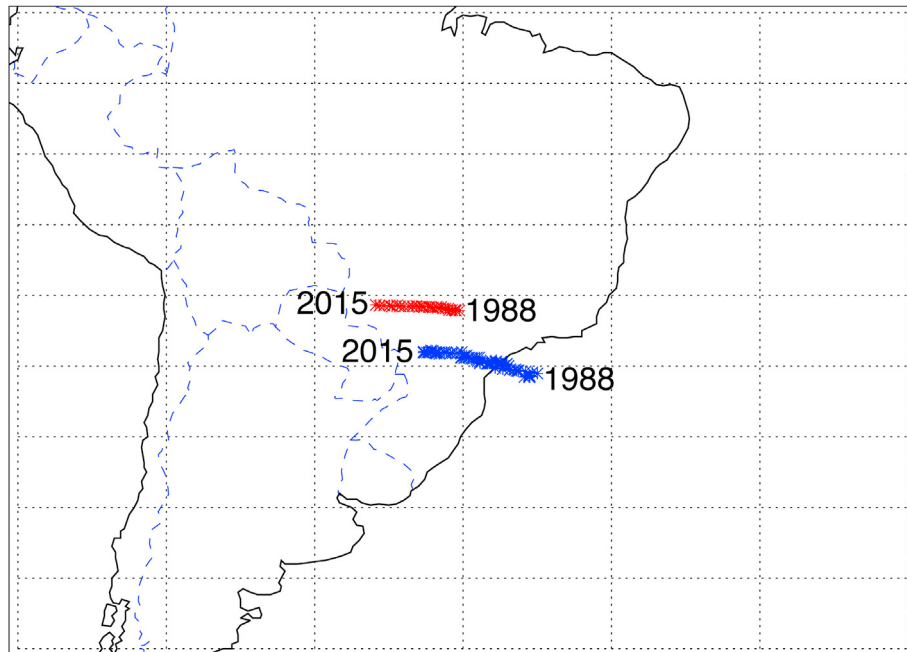


Fig. 14. The identified location of the SAA (blue asterisks) and the location of the minimum in the magnetic field at 800 km (red asterisks) plotted on a map of South America. (For interpretation of the references to color in this figure legend, the reader is referred to the Web version of this article.)

However, the SSUSI instrument is located on the opposite side/bottom of the spacecraft and Schaefer et al., (2016) estimated that most of the particle noise pulses in the SSUSI instrument are produced by protons greater than about 45 MeV. Thus the contamination in the SSUSI instrument is produced by a different population of particles than the contamination in the SSJ/5 instrument. It is well known (i.e., Jones et al., 2017 and Ye et al., 2017) that the location and movement of the SAA varies significantly with particle energy.

We have focused in this paper on using DMSP MeV particle “measurements” to track the movement of the SAA over nearly three decades but they can also be valuable tools for studying the variation of the intensity and extent of the SAA. This will require careful intercalibration of the instruments and accounting for their degradation over time. As mentioned Section 2, we have the tools for doing this and will provide such an analysis of in the future. These data can also be a valuable tool for tracking the variation in MeV electrons the outer radiation belt. That study is underway and will provide such monitoring over more than three decades.

Acknowledgments

The authors are grateful to the PROBA-V/EPT teams at B-USOC and ESA/Redu for deep involvement in the data acquisition process. S. Borisov also thanks P. Coquay, J. Nijskens, H. Verbeelen, and W. Verschueren at the Belgian Science Policy – Space Research and Applications (BELSPO) for support to the PRODEX project entitled “PROBA-V/EPT – Data Exploitation-Extension”, ESA/PRODEX PEA N°C4000107617, as well as M. Cyamukungu, PI of the EPT, for allowing use of the PROBA-V/EPT data.

References

- Badhwar, G., 1997. Drift rate of the South Atlantic Anomaly. *J. Geophys. Res.* 102, 2343–2349.
- Casadio, S., Arino, O., 2011. Monitoring the South Atlantic Anomaly using ATSR instrument series. *Adv. Space Res.* 48 (6), 1056–1066. <https://doi.org/10.1016/j.asr.2011.05.014>.
- Cyamukungu, M., Beck, S., Borisov, S., Gregoire, G., Cabrera, J., Bonnet, J.L., Nieminen, P., 2014. The Energetic Particle Telescope (EPT) on board PROBA-V: description of a new science-class instrument for particle detection in space. *IEEE Trans. Nucl. Sci.* 61 (6), 3667–3681.
- Fürst, F., Wilms, J., Rothschild, R.E., Pottschmidt, K., Smith, D.M., Lingenfelter, R., 2009. Temporal variations of strength and location of the South Atlantic Anomaly as measured by RXTE. *Earth Planet Sci. Lett.* 281, 125–133.
- Ginet, G.P., Madden, D., Dichter, B.K., Brautigam, D.H., 2007. Energetic proton maps for the South Atlantic Anomaly. In: IEEE Radiation Effects Data Workshop, Waikiki, Hawaii, 23–27 Jul.
- Grigoryan, O.R., Romashova, V.V., Petrov, A.N., 2008. SAA drift: experimental results. *Adv. Space Res.* 41, 76–80.
- Hardy, D.A., Yeh, H.C., Schmitt, L.K., Schumaker, T.L., Gussenoven, M.S., Huber, A., Marshall, F.J., Pantazis, J., 1984. Precipitating Electron and Ion Detectors (SSJ/4) on the Block 5D/Flights 6–10 DMSP Satellites: Calibration and Data Presentation. *Tech. Rep. AFGL-TR-84-0317*, Air Force Geophys. Lab., Hanscom Air Force Base, Mass.
- Jones, A.D., Kanekal, S.G., Baker, D.N., Klecker, B.,Looper, M.D., Mazur, J.E., Schiller, Q., 2017. SAMPEX observations of the South Atlantic anomaly secular drift during solar cycles 22–24. *Space Weather* 15 (1), 44–52. <https://doi.org/10.1002/2016SW001525>.
- Kurnosova, L.V., Kolobyanina, T.N., Logachev, V.I., Razorenov, L.A., Sirokin, I.A., Fradkin, M.I., Aug, 1962. Discovery of radiation anomalies above the South Atlantic at heights of 310–340 km. *Planet. Space Sci.* 9, 513–516.
- McFadden, J.P., Evans, D.S., Kasprzak, W.T., Brace, L.H., Chornay, D.J., et al., 2007. In-flight Instrument Calibration and Performance Verification. *ESA Publications Division*, 277–385.
- Merrill, R.T., McElhinny, M.V., 1983. The Earth's magnetic field, its history, origin, and planetary perspective. In: *Int. Geophys. Series*, vol. 32. Academic Press, San Diego, CA.
- Oberhardt, M.R., Hardy, D.A., Slutter, W.E., McGarity, J.O., Sperry, D.J., Everest, A.W., Huber, A.C., Pantazis, J.A., Pl Gough, M., 1994. The shuttle potential and return electron experiment (SPREE). *Il Nuovo Cimento* 17 (1), 67.
- Schaefer, R.K., Paxton, L.J., Selby, C., Ogorzałek, B.S., Romeo, G., Wolven, B.C., Hsieh, S.-Y., 2016. Observation and modeling of the South Atlantic Anomaly in low Earth orbit using photometric instrument data. *Space Weather* 14, 330–342. <https://doi.org/10.1002/2016SW001371>.
- Stassinopoulos, E.G., Xapsos, M.A., Stauffer, C.A., 2015. Forty-year ‘Drift’ and Change of the SAA. *NASA Goddard Spaceflight Center*. NASA/TM-2015-217547, GSFC-E-DAA-TN28435.
- Underwood, C.I., 1990. In-orbit radiation effects monitoring on the UOSAT satellites. In: *Proc. 4th Annual AIAA/USU Conf. On Small Satellites*, pp. 27–30. August 1990, Logan, Utah, USA.
- Ye, Y., Zou, H., Zong, Q., Chen, H., Wang, Y., Yu, X., Shi, W., 2017. The secular variation of the center of geomagnetic South Atlantic Anomaly and its effect on the distribution of inner radiation belt particles. *Space Weather* 15. <https://doi.org/10.1002/2017SW001687>.